Electronic Supplementary Material (ESI) for Chemical Communications.
This journal is © The Royal Society of Chemistry 2020

Electronic Supplementary Information for

Engineering bunched RhTe nanochains for efficient methanol oxidation electrocatalysis

Ziqiang Wang, Hugang Zhang, Songliang Liu, Zechuan Dai, Peng Wang, You Xu, Xiaonian Li, Liang Wang* and Hongjing Wang*

State Key Laboratory Breeding Base of Green-Chemical Synthesis Technology, College of Chemical Engineering, Zhejiang University of Technology, Hangzhou 310014, P. R. China

E-mails: wangliang@zjut.edu.cn, hjw@zjut.edu.cn

Experimental Section

Reagents and chemicals: Rhodium chloride ($RhCl_3$), Sodium tellurite (Na_2TeO_3), polyvinylpyrrolidone (PVP), hydrazine monohydrate ($N_2H_4 \cdot H_2O$), ammonia solution ($NH_3 \cdot H_2O$) and formic acid were purchased from Aladdin. Nafion 117 solution (5 wt%) was obtained Sigma-Aldrich. All reagents were used as received without further purification.

Preparation of Te NWs： Te NWs were synthesized according to reported literature with minor modifications.[1] In brief, 0.09 g Na_2TeO_3 and 1.0 g PVP were completely dissolved in 35 mL H_2O with strong stirring under room temperature. Subsequently, 3.35 mL $NH_3 \cdot H_2O$ and 1.43 mL $N_2H_4 \cdot H_2O$ were injected into above solution to form transparent solution. Then, the obtained solution was sealed in a 50 mL Tefion-lined stainless steel autoclave and heated at 180 °C for 3 h. After cooling, Te NWs were corrected by centrifugation and washing for five cycles. Finally, the Te NWs were dispersed in 10 mL H_2O for further use.

Preparation of RhTe nanochains： For a typical synthesis, 2 mL $RhCl_3$ solution (20 mM) and 0.2 mL Te NWs solution were firstly mixed in 20-mL vial. Then, 1 mL formic acid was successively injected into the previous solution, which was reacted for 180 min at 80 °C. After finishing, RhTe NCs were obtained by centrifugation and washing with three cycles, followed by drying at 60 °C for 12 h under vacuum.

Material characterizations： Scanning electron microscopy (SEM) was performed to investigate the morphology of the as-obtained samples by ZEISS SUPRA 55 instrument at an accelerating voltage of 5 kV. A transmission electron microscopy (TEM, JEOL-2100F) was used to analyze the microstructure of catalysts at an acceleration voltage of 200 kV. The crystallographic structure of samples was performed by a PANalytical X'Pert Powder X-ray diffractometer using a Cu-Kα radiation X-ray source (λ = 1.54178 Å, 40 kV, 40 mA). The chemical state of samples was investigated by X-ray photoelectron spectroscopy (XPS, Axis Ultra spectrometer) using a monochromated Al-Kα X-ray source (1486.7 eV).

Electrochemical investigation： All electrochemical tests were measured by CHI 660E electrochemical workstation in a three-electrode system. The modified glassy carbon electrode (GCE, 3 mm), Hg/HgO electrode (filled with 1.0 M KOH solution) and clean Pt wire were served as the working electrode, reference electrode and counter electrode,

respectively. The preparation of the working electrode was as follows. The as-obtained catalyst (2 mg) was dispersed in water (0.9 mL) and isopropanol (0.1 mL) to form homogeneous suspension under ultrasonication for 20 min. Then, 5 μL of the ink and 3 μL Nafion (0.5 wt%) were successively deposited onto the GCE, followed by drying. The electrochemically active surface area (ECSA) was estimated from cyclic voltammetry (CV) curves at 50 mV s^{-1} in 1 M KOH using the following equation:[2,3]

$$\text{ECSA} = Q/(q \times m) \qquad (1)$$

where Q is the integration charge of the H desorption peak area, m is the Rh loading on the electrode surface and q is the hydrogen adsorption constants of polycrystalline Rh (220 μC cm^{-2}). The typical MOR polarization curves were recorded by cyclic voltammetry (CV) at a scan rate of 50 mV s^{-1} in 1.0 M KOH containing 1.0 M CH_3OH. Chronoamperometric curves were estimated at 0.6 V in 1.0 M KOH containing 1.0 M CH_3OH. For CO stripping tests, the working electrode was first immersed in a CO-saturated electrolyte for 30 min to achieve the maximum coverage of CO molecules at the potential of 0.03 V. Then, CO-stripping voltammetry was conducted in the potential range between 0.03 and 1.0 V in 1.0 M KOH solution at a scan rate of 50 mV s^{-1}. All potentials were converted to the reversible hydrogen electrode (RHE).

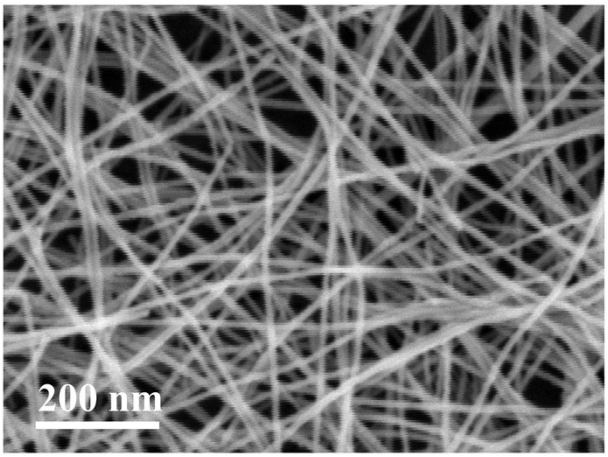

Fig. S1 SEM image of the Te NWs.

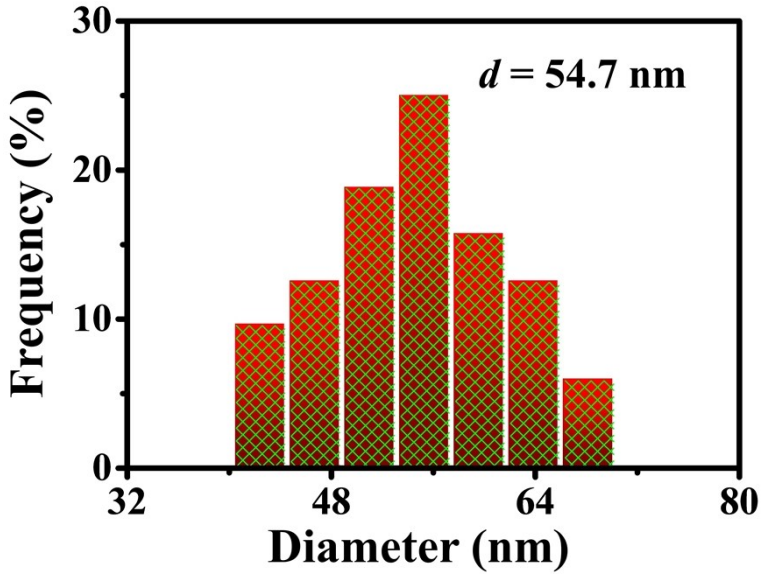

Fig. S2 Histogram of the diameter distribution for RhTe NCs.

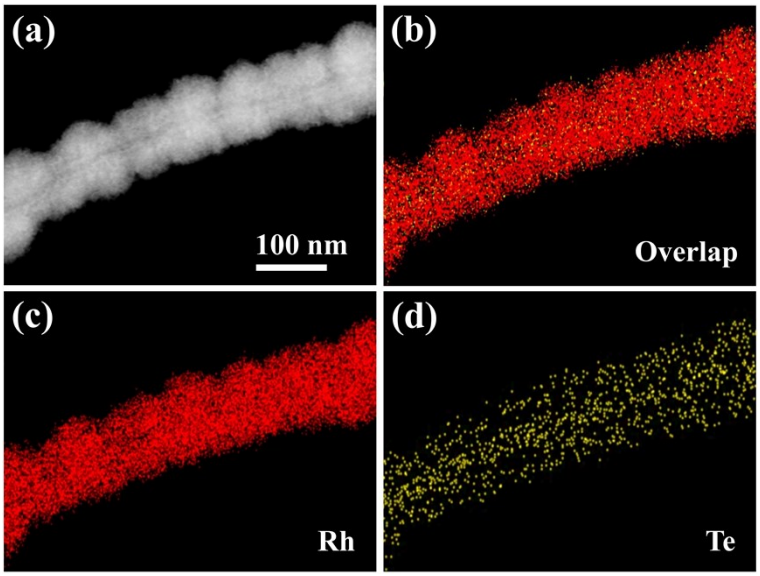

Fig. S3 (a) HAADF-STEM image and (b-e) elemental mapping images of a single RhTe NCs.

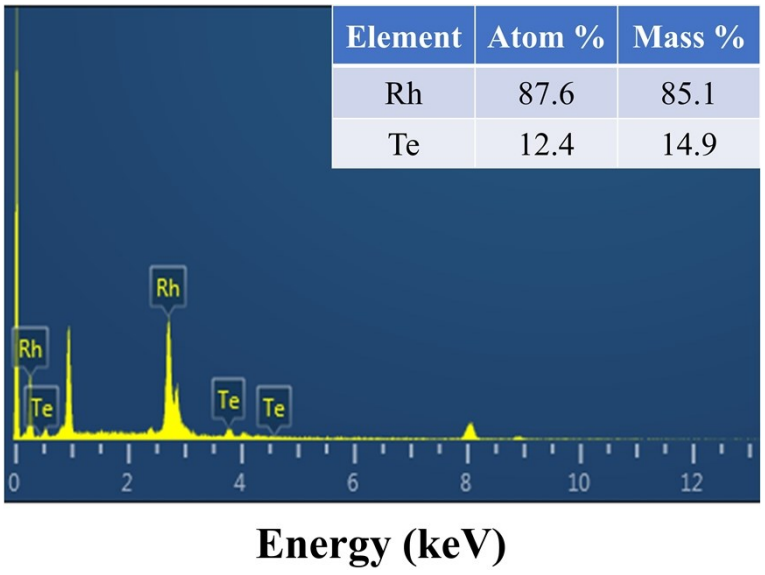

Fig. S4 The EDS spectrum of the RhTe NCs.

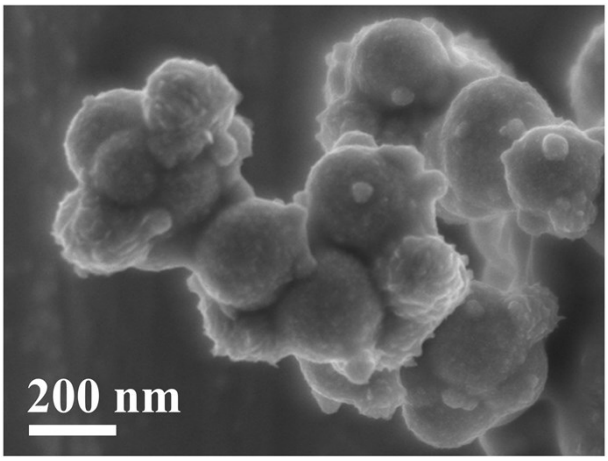

Fig. S5 The SEM image of Rh nanoparticles.

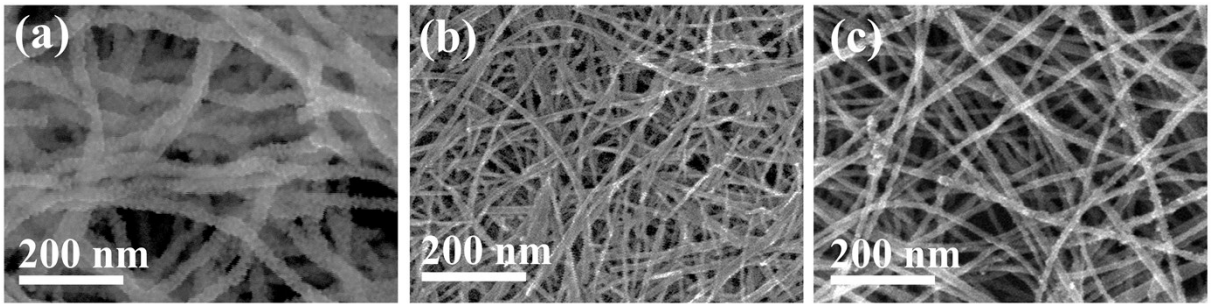

Fig. S6 SEM images of the RhTe NCs obtained without reducing agent (a) and with different reducing agents: (b) acetic acid and (c) 0.1 M AA.

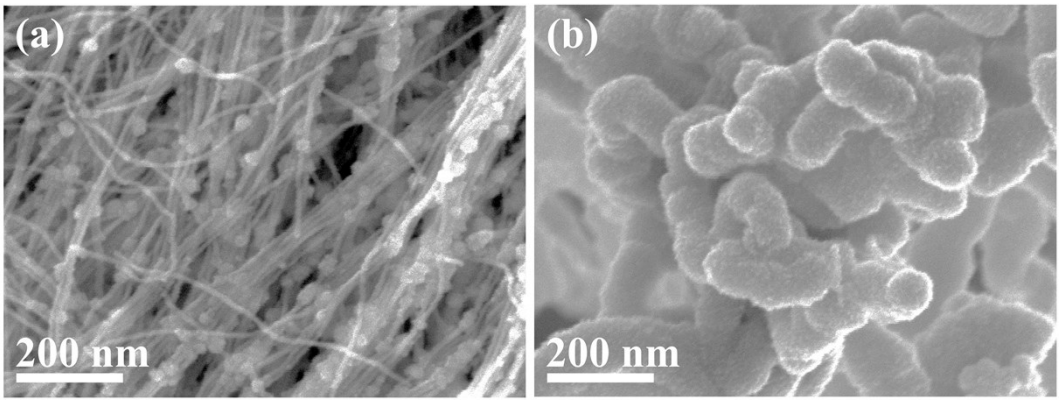

Fig. S7 SEM images of the RhTe NCs prepared with (a) 10 mM, (b) 40 mM of $RhCl_3$.

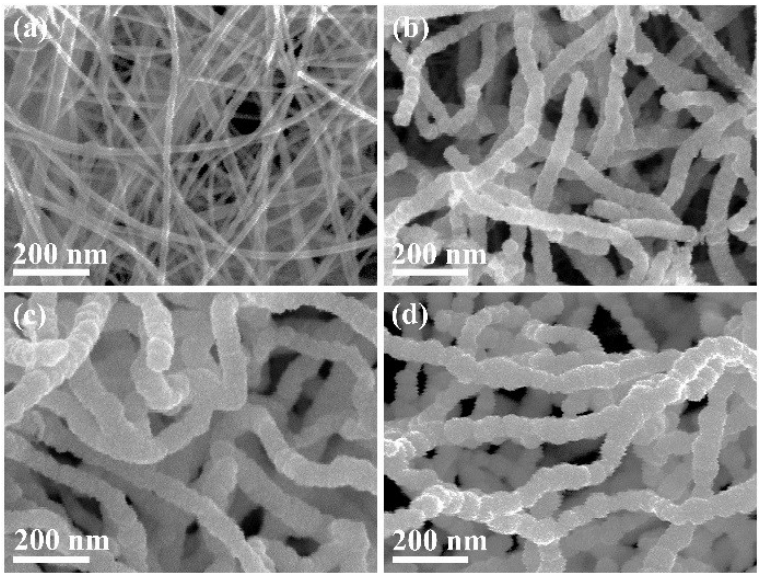

Fig. S8 SEM images of the RhTe NCs obtained at four representative stages during the building-up process: (a) 5 min, (b) 60 min, (c) 120 min, and (d) 180 min.

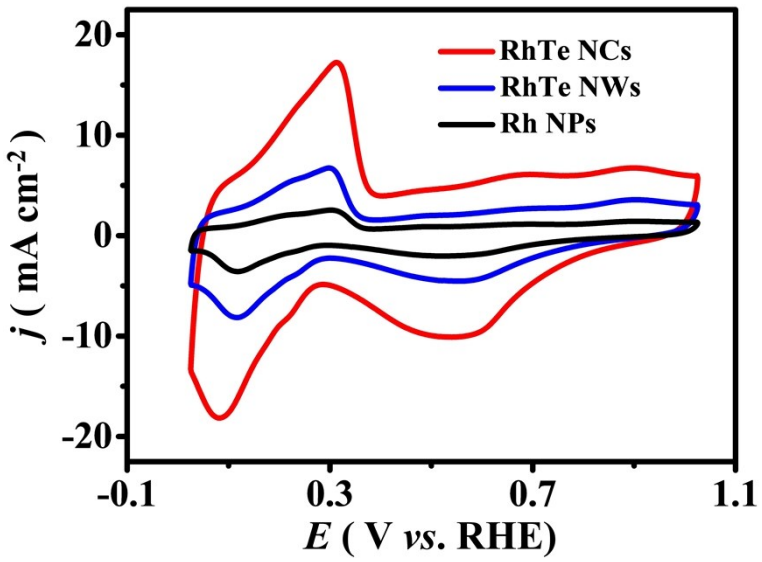

Fig. S9 CVs of the catalysts recorded in a N_2-saturated 1.0 M KOH solution with a scan rate of 50 mV s^{-1}.

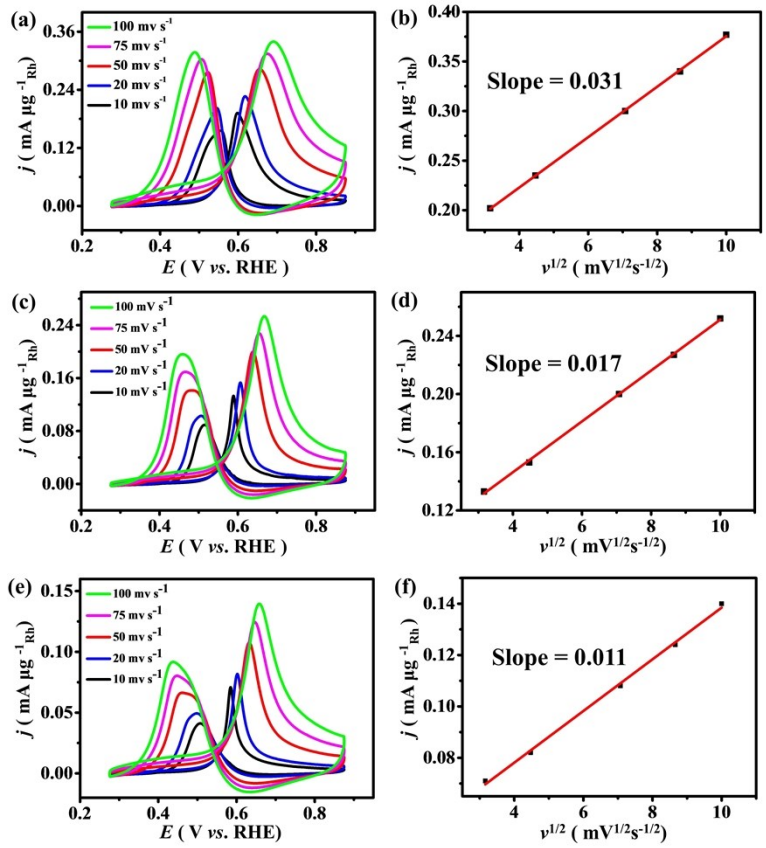

Fig. S10 CV curves of the samples at different scan rates and the corresponding plots of forward peak current (j_m) versus the square root of the scan rate ($v^{1/2}$): (a, b) RhTe NCs, (c, d) RhTe NWs, and (e, f) Rh NPs.

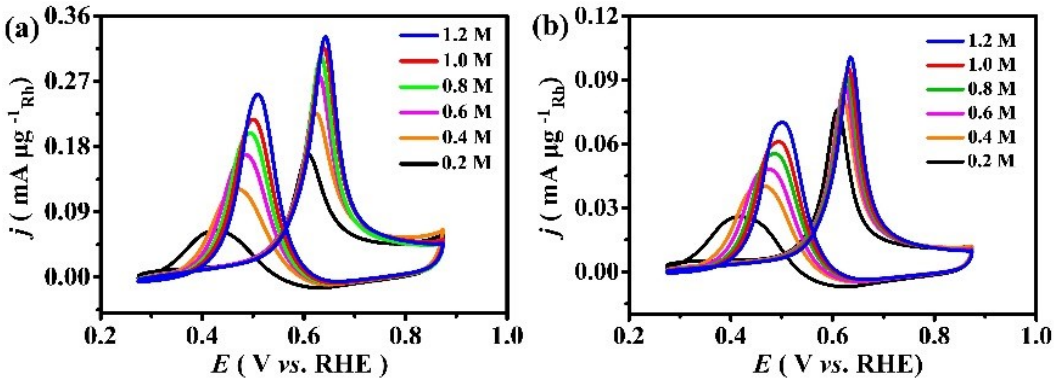

Fig. S11 Cyclic voltammograms in 1.0 M KOH solution in the presence of different concentrations of methanol at a scan rate of 50 mVs^{-1}: (a) RhTe NCs and (b) Rh NPs.

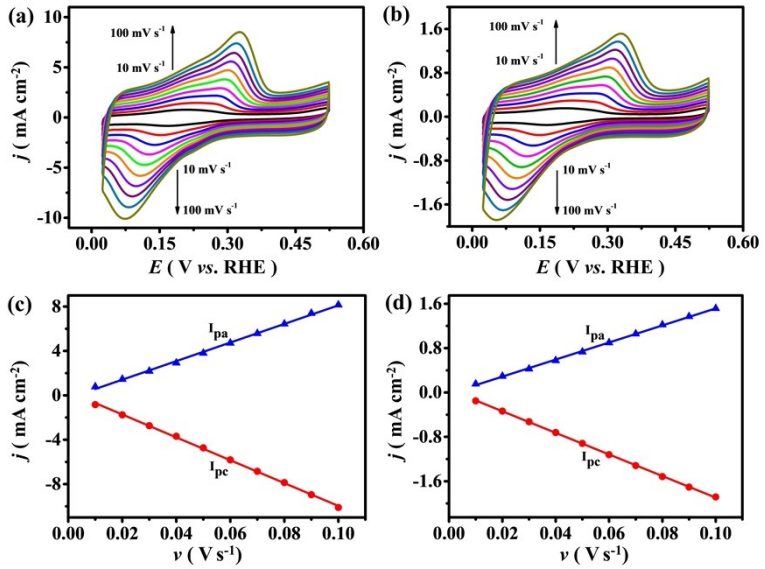

Fig. S12 Cyclic voltammograms in 1.0 M KOH at the different sweep rates: (a) RhTe NCs and (b) Rh NPs. Relationship between the anodic and cathodic peak current densities and the scan rates: (c) RhTe NCs and (d) Rh NPs.

The surface coverage (Γ*) of the RhTe NCs can be calculated according to the following equation:[4,5]

$$Ip = (n^2F^2/4RT)vAI^*$$

where *Ip*, *n*, *R*, *T*, *A*, ν, and I^* are the peak current, the number of transferred electrons, the Faraday constant (96485 C mol^{-1}), the general gas constant (8.314 J K^{-1} mol^{-1}), the thermodynamic temperature, the apparent area of the electrode, the potential scan rate, and the surface coverage of the redox species, respectively. Fig. S13a shows CV curves of the RhTe NCs in 1.0 M KOH solution at different scan rates from 10 to 100 mV s^{-1}. The anodic and the cathodic peak current densities increased with the increase of scan rate. As shown in Fig. S13b, the anodic and the cathodic peak current densities (*Ipa* and *Ipc*) of the RhTe NCs exhibited a linearly proportional to the scan rate (ν). Therefore, the surface coverage (I^*) of redox species for the RhTe NCs was calculated to be 1.28 × 10^{-6} mol cm^{-2} according to the average of the anodic and the cathodic results. For comparison, the value of I^* for Rh NPs was obtained to be 2.27 × 10^{-7}. Obviously, the RhTe NCs electrocatalyst exhibited a significantly larger surface coverage of redox species I^*, which is approximately 5-fold higher than that calculated for the Rh NPs.

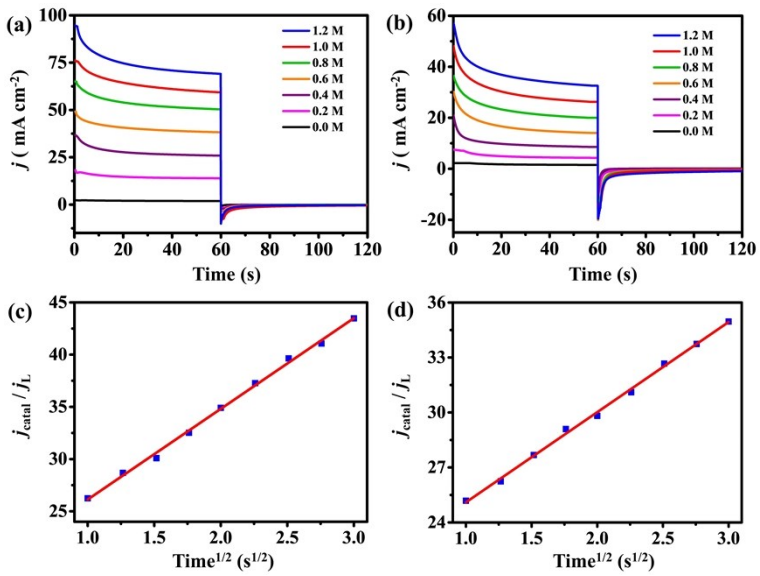

Fig. S13 Double potential step chronoamperometry curves of the as-obtained samples: (a) RhTe NCs and (b) Rh NPs in 1.0 M KOH solution with different concentrations of methanol ranging from 0 to 1.2 M. Potential steps are 0.6 V and 0 V. Dependence of j_{catal}/j_L on $t^{1/2}$ for (c) RhTe NCs and (d) Rh NPs derived from the data of double potential step chronoamperometry curves of in presence of 1.0 M methanol and in absence of methanol.

Zhang et al.[6] proposed the use of chronoamperometric technique for evaluation of the catalytic rate constant in accordance with the equation:

$$j_{catal}/j_L = \lambda^{1/2}[\pi^{1/2} erf\,(\lambda^{1/2}) + \exp(-\lambda)/\lambda^{1/2}]$$

where j_{catal} and j_L are the currents in the presence and absence of methanol and $\lambda = kC^*t$ is the argument of the error function. k is the catalytic rate constant, C^* is bulk concentration of methanol and t is elapsed time (s). For $\lambda > 1.5$, $erf\,(\lambda^{1/2})$ almost equals unity and $exp(-\lambda)/\lambda^{1/2}$ is so small and the above equation can be reduced to:

$$j_{catal}/j_L = \lambda^{1/2}\pi^{1/2} = \pi^{1/2}(kC^*t)^{1/2}$$

According to the slope of the j_{catal}/j_L *vs* $t^{1/2}$, the catalytic rate constant k is estimated to be 2.401×10^4 and 0.771×10^4 $cm^3\ mol^{-1}\ s^{-1}$ for RhTe NCs and Rh NPs, respectively.

Table S1 The mass activity comparison of alcohol oxidation on various Rh-based electrocatalysts in alkaline media.

Catalysts	Condition	Scan rate ($mV\ s^{-1}$)	Mass activity ($A\ mg^{-1}_{Rh}$)	Ref.
RhTe NCs	**1.0 M KOH containing 1.0 M CH_3OH**	**50**	**0.317**	**This work**
Rh Nanodendrites	1.0 M KOH containing 1.0 M CH_3CH_2OH	50	0.2556	7
Rh-NSs/RGO Hybrids	1.0 M KOH containing 1.0 M CH_3OH	50	0.264	8
Rh_3Co_1/CB Nanohybrids	1.0 M KOH containing 1.0 M CH_3OH	50	0.3065	9
N-MRhS	1.0 M KOH containing 1.0 M CH_3OH	50	0.722	9
S-MRhS	1.0 M KOH containing 1.0 M CH_3OH	50	0.27	10
Mesoporous Rh	1.0 M KOH containing 1.0 M CH_3OH	50	0.288	11
Hollow Porous Rh Nanoballs	1.0 M NaOH containing 1.0 M CH_3CH_2OH	50	0.0786	12
Rh H-NSs	1.0 M KOH containing 1.0 M CH_3OH	50	0.292	13
HP-Rh NSs	1.0 M KOH containing 0.5 M CH_3OH	50	0.333	14
Pt_1Rh_1 ANDs	1.0 M NaOH containing 1.0 M CH_3CH_2OH	50	0.4621	15
Ultrafine Wavy Rh Nanowires	1.0 M KOH containing 1.0 M CH_3OH	50	0.722	16

References

1 S.-Y. Ma, H.-H. Li, B.-C. Hu, X. Cheng, L. Q.-Q Fu, S.-H. Yu, *J. Am. Chem. Soc.*, 2017, 139, 5890-5895.

2 T.H.M. Housmans, J.M. Feliu, M.T.M. Koper, *J. Electroanal. Chem.*, 2004, 572, 79-91.

3 Y. Kang, Q. Xue, P. Jin, J. Jiang, J. Zeng, Y. Chen, *ACS Sustainable Chem. Eng.*, 2017, 5, 10156-10162.

4 X. Cui, P. Xiao, J. Wang, M. Zhou, W. Guo, Y. Yang, Y. He, Z. Wang, Y. Yang, Y. Zhang, Z. Lin, *Angew. Chem., Int. Ed.,* 2017, **129**, 4559-4564.

5 X. Cui, W. Guo, M. Zhou, Y. Yang, Y. Li, P. Xiao, Y. Zhang, X. Zhang, *ACS Appl. Mater. Interfaces,* 2015, **7**, 493-503.

6 X. Cui, Y. Yang, Y. Li, F. Liu, H. Peng, Y. Zhang, Peng Xiao, *J. Electrochem. Soc.*, 2015, **162**, F1415-F1424.

7 Y. Kang, F. Li, S. Li, P. Ji, J. Zeng, J. Jiang, Y. Chen, *Nano Res.,* 2016, **9**, 3893-3902.

8 Y. Kang, Q. Xue, P. Jin, J. Jiang, J. Zeng, Y. Chen, *ACS Sustainable Chem. Eng.,* 2017, **5**, 10156-10162.

9 Y.-N. Zhai, Y. Li, J.-Y. Zhu, Y.-C. Jiang, S.-N. Li, Y. Chen, *J. Power Sources,* 2017, **371**, 129-135.

10 Y. Guo, S. Chen, Y. Li, Y. Wang, H. Zou and X. Tong, *Chem. Commun.,* 2020, **56**, 4448-4451.

11 B. Jiang, C. Li, O. Dag, H. Abe, T. Takei, T. Imai, M.S.A. Hossain, M.T. Islam, K. Wood, J. Henzie, Y. Yamauchi, *Nat. Commun.* 2017, **8**, 15581.

12 J. Zhang, Y. Jiang, S. Shi, H. Li, J. Chen, Q. Kuang, Z. Xie, L. Zheng, *Chem. Commun.,* 2019, **55**, 4989-4952.

13 Y.-Q. Kang, Q. Xue, Y. Zhao, X.-F. Li, P.-J. Jin, Yu Chen, *Small,* 2018, **14**, 1801239.

14 J.-Y. Zhu, S. Chen, Q. Xue, F.-M. Li, H.-C. Yao, L. Xu, Y. Chen, *Appl. Catal., B,* 2020, **264**, 118520.

15 J. Bai, X. Xiao, Y.-Y. Xue, J.-X. Jiang, J.-H. Zeng, X.-F. Li, Yu Chen, *ACS Appl. Mater. Interfaces,* 2018, **10**, 19755-19763.

16 L. Gong, Z. Yang, K. Li, W. Xing, C. Liu, J. Ge, *J. Energy Chem.,* 2018, **27**, 1618-1628.